HAMSTIR

High Amplitude Moon Surface Telecommunication Inflatable Repeater

Kathryn Soderman[1], Brennan Donovan[2], James Fernandez[3], Jason Solomon[4], Nate VanDermark[5], Sam Masten[6], Vennela Gottiparthy[7]
North Carolina State University, Raleigh, NC, 27606, US

As humanity continues to embark on ambitious space exploration endeavors, establishing robust communication networks on celestial bodies such as the Moon becomes increasingly critical. Traditional Earth-based cell towers are unsuitable for lunar missions due to payload limitations. The High Amplitude Moon Surface Telecommunications Inflatable Repeater (HAMSTIR) project addresses this challenge by introducing an innovative solution.

HAMSTIR serves as a lightweight and deployable RF repeater tower, engineered to amplify and relay 4G signals between base stations, user devices, and other HAMSTIR units. Leveraging Nokia's 4G core network partnership with NASA, HAMSTIR aims to extend communication coverage on the Moon, facilitating seamless connectivity for astronauts and rovers alike. Central to HAMSTIR's design is its telescoping inflatable structure, meticulously crafted to optimize deployment efficiency by inflating sectionally so that it can sit in a compact and collapsed state, minimizing payload requirements such as mass and volume. A cable tensioning mechanism enhances structural stability during deployment, ensuring the tower's integrity in lunar conditions. Additionally, HAMSTIR is equipped with a multi-layered protective coating to shield it from extreme temperatures and radiation, enhancing its durability and longevity on the lunar surface.

HAMSTIR's communication equipment is powered by solar panels mounted on the base box, providing a sustainable energy source for prolonged operations. Astronauts oversee the deployment process, aligning the tower for optimal signal reception and strategically distributing multiple towers to enhance coverage across the lunar landscape.

HAMSTIR represents a significant advancement in lunar telecommunications, laying the groundwork for enhanced communication infrastructure essential for the success of future lunar missions. This paper highlights the importance of innovation in driving sustainable space exploration endeavors forward, underscoring the transformative potential of projects like HAMSTIR in advancing humanity's reach into the cosmos.

I. Introduction

Humanity's quest to explore and expand its presence beyond Earth has entered a new era of ambitious space exploration endeavors. As missions to celestial bodies like the Moon become increasingly frequent and complex, the need for robust communication infrastructure in extraterrestrial environments becomes ever more critical. Traditional Earth-based communication systems are ill-suited for lunar missions due to the challenges posed by the lunar landscape and the limitations of existing technology.

In response to these challenges, the HAMSTIR project emerges as a pioneering initiative aimed at revolutionizing communication infrastructure for lunar exploration missions. By introducing innovative solutions that integrate inflatable structures, telecommunications, power systems, structural mechanics, and thermal considerations, HAMSTIR seeks to address the unique challenges of establishing communication networks on the Moon.

This paper provides a comprehensive overview of the HAMSTIR project, outlining its interdisciplinary approach and detailing the design, analysis, and testing methodologies employed to develop this groundbreaking technology.

---

[1]Project Manager, Aerospace Engineering, Undergraduate, Student Member, 1600882
[2]Inflation Systems Engineer, Aerospace Engineering, Undergraduate, Student Member, 1315065
[3]Structures and Mechanisms Engineer, Aerospace Engineering, Undergraduate, Student Member, 1597533
[4]Communications Systems Engineer, Aerospace Engineering, Undergraduate
[5]Structures and Mechanisms Engineer, Aerospace Engineering, Undergraduate, Student Member, 1326452
[6]Power and Electrical Engineer, Aerospace Engineering, Undergraduate, 1605590
[7]Thermal, Radiation, and Survivability Engineer, Aerospace Engineering, Undergraduate, Student Member, 1230762

From the conceptualization of mission objectives to the refinement of prototype designs through iterative reviews and simulations, every aspect of HAMSTIR's development process is meticulously examined and evaluated.

Through collaborative efforts and innovative engineering, the HAMSTIR project aims to bridge the gap between the Earth and the lunar surface, providing uninterrupted connectivity for astronauts, rovers, and exploration assets. HAMSTIR's innovative design and development marks a significant leap in lunar telecommunications, paving the way for expanded connectivity and support for forthcoming lunar missions. As HAMSTIR's prototype approaches completion and enters extensive testing phases, this paper highlights the transformative impact such initiatives have on propelling sustainable space exploration. Through promoting innovation and fostering collaboration, HAMSTIR sets the stage for a new era of lunar communication infrastructure, amplifying humanity's reach and knowledge of the cosmos.

II. Methodology

The design of HAMSTIR integrates a multidisciplinary approach, drawing upon expertise from multiple different subsystems. These subsystems include inflatable structures, telecommunications, structures and mechanisms, power and electrical, and thermal, radiation, and survivability. Initially, conceptual designs were generated based on mission objectives, payload constraints, and technological feasibility. Iterative design reviews were conducted to refine the conceptual models for prototyping, incorporating feedback from stakeholders and subject matter experts. Critical design considerations included optimizing the inflatable structure for deployment efficiency, minimizing payload volume and mass, and ensuring structural integrity and stability in lunar conditions. Material selection, component integration, and compatibility with future lunar infrastructure, such as Nokia's 4G LTE network, were also key factors guiding the design process.

The deployment procedures for HAMSTIR were meticulously planned to facilitate seamless and reliable deployment on the lunar surface. A step-by-step deployment sequence was established, detailing the actions required by astronauts to deploy the tower from its stowed configuration to its operational state. Upon arrival at the lunar surface, astronauts would initiate the deployment process by connecting a nitrogen tank to the pressure valve of the base box containing HAMSTIR. Solar panels are then deployed to provide power to the communication equipment. Subsequently, the antenna mount is attached to the top of the deflated tower where communication and power cables are connected. The mount is then rotated to align the receiving antenna with the Nokia base tower. The inflation process begins with the top section of the tower and proceeds sequentially downwards. Cable tensioners attached to the basebox deploy and retract accordingly to ensure vertical deployment, while triangular slot bearing supports extend vertically and lock into place within the inflatable portion of the tower to provide stability and structural support. Throughout the deployment, astronauts oversee the process, ensuring proper alignment and functionality of the tower components.

Operational testing of HAMSTIR involves comprehensive verification and validation procedures to assess performance under simulated lunar conditions. Testing protocols encompass functional, environmental, and system integration. Functional testing evaluates the operational capabilities of HAMSTIR, including signal amplification, transmission reliability, and power efficiency. Environmental testing assesses the system's resilience to lunar temperatures, radiation, and vacuum conditions. System integration testing verifies interoperability with existing lunar infrastructure and compatibility with communication protocols. System analysis was also performed analytically and with MATLAB and ANSYS simulations to inform optimized iterative design improvements and confirm conceptual feasibility of each subsystem.

A. Communications Subsystem Analysis

The HAMSTIR communications system comprises three key components: a parabolic antenna for long-range communication with base stations, a sector antenna for mobile device connectivity, and a bi-directional amplifier for signal processing. The prototype HAMSTIR will feature a simplified cellular setup with a wifi repeater and a 3D printed rotating cellular mount, showcasing functionality with reduced complexity.

There are three main critical points in the HAMSTIR communications subsystem that were analyzed and simulated in order to ensure the system's feasibility. The first has to do with antenna isolation, which is paramount to prevent signal interference and can significantly degrade performance or even cause system failure. Equation (1) quantifies isolation amplitude, I, by considering factors such as separation distance, d, and antenna gain, G. Achieving adequate isolation ensures that signals remain distinct and unaffected by neighboring antennas, thereby maintaining optimal communication quality. Typically for 4G cellular systems, an isolation amplitude of at least 10 dB is required for low interference [11]. Physically separating antennas in the vertical direction is much more efficient than in the horizontal plane, and significantly lowers the required separation distance to achieve isolation.

$$I = 28 + 40 * log10(\frac{d}{\lambda}) - G \quad (1)$$

The second critical aspect assesses the HAMSTIR's transmission range to ensure adequate signal strength for reliable mobile network connectivity. For 4G networks, a signal strength of -110 dBm indicates satisfactory connectivity [11]. Accounting for signal attenuation over distance, the Friis Transmission Equation, as shown in Eq. (2) evaluates the received signal strength by considering path loss, antenna gains, and repeater gain [12].

$$P_{MS} = P_{RX} + G_{RX} + G_{TX} + G_{BDA} - 20 * log10(\frac{4*\pi*d}{\lambda}) \quad (2)$$

Where P_{MS} is the power received by the mobile station using the network in dB, P_{RX} is the power received by the tower dB, G_{RX} is the gain of the tower receiving antenna in dB, G_{TX} is the gain of the tower transmitting antenna in dB, G_{BDA} is the gain of the bi-directional amplifier in dB, d is the mobile station distance from the tower in ft, and λ is the wavelength of the signal in ft. The third critical aspect concerns the moment balance of the entire cellular subsystem around the tower's center. Balancing these moments ensures the tower remains upright during inflation, evenly distributing loads on rigid structures once fully deployed. Individual component moments were calculated and summed to determine the overall moment around the tower's center. This is shown below in Eq. (3).

$$\Sigma M_{center} = 0 = M_{PA} + M_{R} - M_{SA} - M_{WR} - M_{H} \quad (3)$$

Where M_{center} is the moment about the center of the tower, M_{PA} is the moment due to the parabolic antenna, M_R is the moment due to the securement rod, M_{SA} is the moment due to the sector antenna, M_{WR} is the moment due to the wire rope, and M_H is the moment due to the hanger bar that the wire rope is attached to.

B. Inflation Subsystem Analysis

For the full-scale modeling of the HAMSTIR tower, we analyzed the inflation and stability of a silicone bladder under lunar conditions. The prototype will be assembled utilizing a vinyl inflatable to show proof of concept. In both models, each section is separated via the sphincter system. A thin film with a central hole limits airflow to encourage sectional inflation providing a more structurally stable deployment.

One of the equations that was used for the inflation system was the ideal gas law referenced as Eq. (4b) below. To find the force acting on the inflatable bladder and the overall inflatable section, we used Hooke's Law in Eqs. (4) and (5) shown below. Where σ is the stress, V is the volume, A is the cross sectional area of the structure being analyzed, ε is the strain, and E is the young's modulus of the material.

$$\sigma_{max} = (\frac{n_{max} RT_{max}}{V})/A \quad (4)$$

$$F = \frac{\sigma}{A} \quad (4a)$$

$$PV = nRT \quad (4b)$$

$$E = \sigma/\varepsilon \quad (5)$$

To comprehensively assess the tower's structural integrity, we used MATLAB to ascertain the required nitrogen volume within the tower, considering the pressure exerted by the communications equipment. By plotting pressure against varying temperatures, a range of nitrogen mole quantities necessary to maintain pressure was obtained and we found the minimum number of moles of nitrogen, n_{max} , to be 1.3856e6. This analysis ensured consistent tower performance across temperature fluctuations. To determine the range of the tower's capabilities, the maximum number of moles it could hold is 1.438e12, giving a substantial factor of safety and assurance that the tower can endure the lunar environment. This systematic approach evaluated the feasibility and performance of the inflation subsystem in the HAMSTIR system.

C. Power and Electrical Subsystem Analysis

The full-scale HAMSTIR design components are four large, space-grade silicon solar cells to generate power during the lunar day cycles, a 24V, 400Ah LiFeP04 industrial lithium-ion battery to store power for lunar night cycles, and an MSP430 microcontroller to minimize power consumption. The prototype model will have two small monocrystalline solar panels and a 12V, 5200 mAh lithium-ion battery pack, but no microcontroller due to a much lower power consumption.

The power and electrical subsystem of the full-scale HAMSTIR system was analyzed to ensure efficient power management and reliable electrical performance. Key aspects of this analysis include average power consumption calculations, battery capacity calculations, solar power analysis, battery life calculations, and charge and discharge time calculations. To analyze the battery life cycle, a number of equations are required. The first of these is the average power rating equation. This equation factors the ratio of time the HAMSTIR spends in the respective power consumption modes as shown in Eq. (6).

$$P_{average} = \frac{(P_{idle} * ratio_{idle}) + (P_{active} * ratio_{active})}{ratio_{total}} \quad (6)$$

Where $P_{average}$ is the average power consumption in Watts, P_{idle} is the power consumption in idle mode in Watts, P_{active} is the power consumption in active mode in Watts, $ratio_{idle}$ is the ratio of time spent in idle mode, $ratio_{active}$ is the ratio of time spent in active mode, and $ratio_{total}$ is the ratio of overall time. With average power calculated, the battery specifications can be found. The first of these is the battery capacity, which effectively shows how long a battery can deliver a specific current for [13] as seen in Eq. (7) below.

$$C = \frac{P}{V} * t \quad (7)$$

Where C is the battery capacity in Ah, P is the power draw in Watts, V is the battery voltage in Volts, and t is the duration of battery use in hours.The energy stored in the battery in Wh can be calculated using Eq. (8), as shown below. This equation signifies the rated energy capacity of the battery where, E is the battery energy capacity in Wh. Similarly, to calculate the energy capacity drawn from the battery, Eq. (9) is used where E is the battery energy capacity drawn from the battery in Wh.

$$E_{rating} = C * V = P * t \quad (8)$$

$$E_{draw} = P * t \quad (9)$$

Ideally, the rated energy capacity should be higher than the energy drawn from the battery. In other words, E_{draw} should be less than E_{rating}. If it is not, the battery does not have sufficient capacity to power the battery for the required draw duration. To generate accurate simulations of the battery cycle, the most important equation is that of the battery life, as shown below in Eq. (10). This equation yields the duration, in hours, that a battery of capacity rating E can provide a constant power draw of $P_{average}$.

$$Life = \frac{E}{P_{average}} \quad (10)$$

The last equation used in the battery simulations is the charge and discharge time equation where, $t_{charge/discharge}$ is the time in hours needed to charge or discharge the battery. The current charging/discharging rating can vary, and thus the battery voltage and average power draw can also be used to calculate the charge and discharge time assuming a constant power draw. This is shown below in Eq. (11).

$$t_{charge/discharge} = \frac{C}{I} = \frac{C * V}{P} \quad (11)$$

To analyze the solar panel efficiency and power output we used the power output equation which yields the power output that one should expect for a solar panel with known power rating and efficiency, as shown below in Eq. (12). Here, P_{out} is the power output in Watts, η is the solar panel efficiency value between 0.00 and 1.00, and P_{rating} is the wattage rating of the solar panel in Watts. The solar irradiance equation, as shown in Eq. (13), was also used to obtain the required power generation where E is the solar irradiance in Watts per square meter, and A is the area in square meters.

$$P_{out} = \eta * P_{rating} \tag{12}$$

$$P_{out} = \eta EA \tag{13}$$

D. Structures and Mechanisms Subsystem Analysis

The structures and mechanisms subsystem methodology involves analyzing stress, strain, and mass contributions of each component. Hooke's Law was applied to prevent catastrophic deformations or breaks and resultant analysis on the Young's Modulus was conducted. Mass contributions were determined using material density and structure volume, as shown in Eq. (14).

$$m = \rho * V \tag{14}$$

Next, the stress and strain on the components were evaluated using Hooke's Law to ensure structural integrity. If the loads exceed the tensile or shear strength of materials, it could lead to failures. The main focus was on analyzing the stress and strain on the support structure rods to ensure the tower's safety. Additionally, each component's contribution to the overall load on the base box was analyzed to maintain stability. This analysis was done while keeping in mind that the summation of forces must equal zero to ensure structural static stability.

In the full-scale design, it was determined that Aluminum 6061-T6 would be used for each portion of the design due to its low density of $2700\ kg/m^3$ and moderate tensile strength of around 290 MPa. In the prototype design, plexiglass was used for the basebox due to its low density of $1190\ kg/m^3$ and strong tensile strength of around 70 MPa. ABS filament was used for the entire tri-slot design featuring similar characteristics with a density of about $1100\ kg/m^3$ and a tensile strength of 65 MPa.

E. Thermal, Radiation, and Survivability Subsystem Analysis

The thermal, radiation, and survivability subsystem of the HAMSTIR system is crucially evaluated to ensure effective thermal management and survivability. Critical properties of this subsystem such as thermal conductivity, specific heat capacity, porosity, and reflective coating properties are meticulously evaluated for effective heat resistance and management. This evaluation determined the material layering for both the full-scale tower and the small-scale prototype. The full-scale tower comprised a silicone bladder core, surrounded by Kevlar for strength, Nextel ceramic fiber for heat protection, Kapton polyamide film for radiation shielding, and an outer layer of vapor-deposited aluminum for solar reflectance. In contrast, the small-scale prototype substituted silicone with vinyl due to budgetary constraints, maintaining Kevlar as the surrounding layer.

For effective heat resistance, properties like thermal conductivity and specific heat capacity are vital. Thermal conductivity of the outermost materials should be high to resist heat effectively. Equations (15) and (16) were used to calculate thermal conductivity and specific heat capacity, where k represents thermal conductivity, Q denotes heat transferred, d stands for sample thickness, A represents surface area, ΔT indicates change in temperature, and C is the specific heat capacity. A lower specific heat capacity was preferred for the inflatable materials so that they are less likely to retain excessive heat.

$$k = \frac{Qd}{A\Delta T} \tag{15}$$

$$Q = mC\Delta T \tag{16}$$

Porosity, particularly for the silicone inflatable bladder, is crucial to calculate, aiming for minimal air escape from the materials. Equation (17) was employed for porosity calculation, with P representing porosity as a decimal (between 0 and 1), V_v denoting the volume of pores or voids in the material, and V_t indicating the total volume of the material.

$$P = \frac{V_v}{V_t} \tag{17}$$

To assess the tower's structural integrity, Hooke's Law (Eq. ()) was employed. The most brittle material, Nextel ceramic fiber, was chosen to gauge the composite's limit due to its susceptibility to failure under extreme conditions. With a Young's Modulus of 37.7e6 psi, its brittle nature was accentuated. This facilitated the determination of the material's limit using Hooke's Law.

Dielectric strength (D) and insulation resistance (IR) determine material electrical resistance. Greater values are desirable for withstanding higher electrical fields and current flow resistance. Equation (18) calculates dielectric strength using the voltage at which electrical failure occurs (Vb), while Eq. (19) computes insulation resistance (IR) based on the current flowing through the material (I).

$$D = \frac{V}{d} \tag{18}$$

$$IR = \frac{V}{I} \tag{19}$$

The Fresnel Equations are relevant to reflectance, which is a high priority property for the outer Vapor-deposited aluminum coating. The Fresnel equations describe how light is reflected and refracted and are used to calculate the intensity of reflected light. For perpendicular polarization and parallel polarization calculations, Eqs. (20) and (21) were used.

$$\text{perpendicular polarization: } r_p = (n_1 * \cos(\theta_i) - n_2 * \cos(\theta_t)) / (n_1 * \cos(\theta_i) + n_2 * \cos(\theta_t)) \tag{20}$$

$$\text{parallel polarization: } r_s = (n_2 * \cos(\theta_i) - n_1 * \cos(\theta_t)) / (n_2 * \cos(\theta_i) + n_1 * \cos(\theta_t)) \tag{21}$$

Where r_p is the reflection coefficient for p-polarized light, n_1 is the refractive incident of the incident medium, n_2 is the refractive index of the transmitting medium, θ_i is the angle of incidence, and θ_t is the angle of refraction, and r_s is the reflection coefficient for s-polarized light.

III. Results

A. Communications Subsystem

Results for the HAMSTIR project's communication subsystem were obtained through MATLAB simulations, yielding critical insights into antenna isolation, Friis transmission, and moment balance. The results from the analysis of antenna isolation from Eq. (1) revealed that a vertical separation distance of 5.81087 ft achieves an isolation amplitude of 10 dB, meeting our design requirements. To ensure minimal interference, a safety factor was included, resulting in a 6 ft separation distance, facilitating simultaneous signal transmission and reception without performance loss.

For the Friis transmission analysis, solving Eq. (2) in MATLAB showed that the HAMSTIR can extend signal coverage over 1.40883 km, surpassing our initial design requirements. This demonstrates the HAMSTIR's capability to boost weak signals for reliable mobile connectivity.

For the moment balance, MATLAB simulations using Eq. (3) determined the optimal placement of the parabolic antenna and its securement rod relative to the HAMSTIR's center for achieving a zero moment. Using aluminum 6061 alloy for mounting structures and wire rope, and specifying masses for the antennas, the distance to the parabolic antenna securement rod center was found to be 0.34389 ft. This crucial finding was integrated into our CAD models to ensure precise alignment of the communication subsystem's center of mass with the HAMSTIR's center.

B. Inflation Subsystem

The main focus of our inflation system testing was validating the implementation of a design solution that would allow the HAMSTIR to inflate sectionally, encouraging a more stable deployment by enhancing the stability and structural integrity. To encourage the tower to inflate sectionally, each layer of the inflatable bladder has a thin film to separate each other with a small center hole. Figure (1), as shown below, depicts the interior of the full-scale space-grade tower model, illustrating the various "sphincters" that are being utilized to differentiate each section allowing for pressure build up in each section.

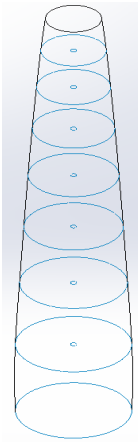

Fig.1 Sphincter System for Full-Scale Model

Using ANSYS Fluent, we conducted a detailed 2D axisymmetric transient simulation to assess the functionality of the proposed inflation system. This simulation was used to determine how efficient the sphincter method would be at encouraging air movement to circulate within sections as opposed to homogeneously. Figure (2) captures both the intricate mesh structure and the corresponding pressure distribution obtained through our simulation of our small-scale prototype. The simulation below was created based on approximations from our air tank to get a pressure differential across each section of the tower. The geometry pictured in the figure shows a 2D cross-sectional representation of the HAMSTIR tower and is pictured with the base of the inflatable portion of the tower on the left and the top layer of the tower on the right.

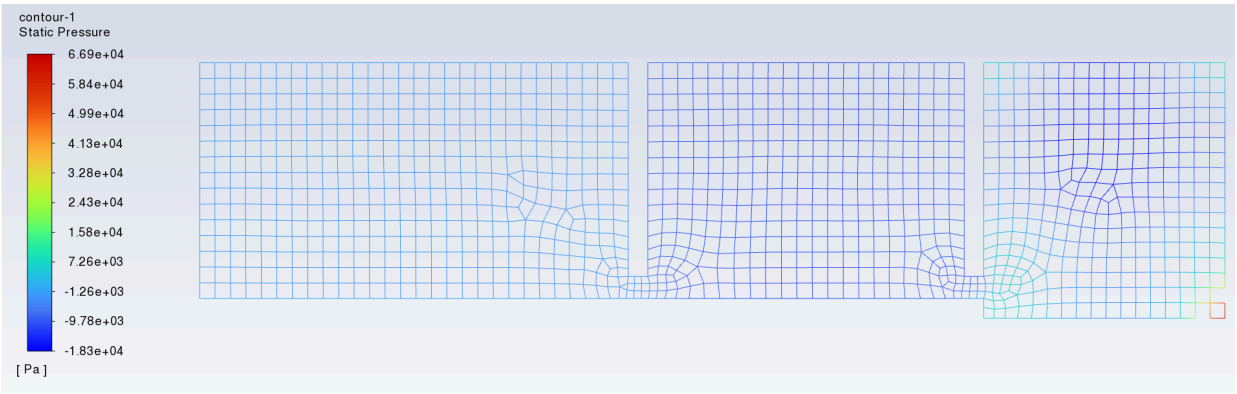

Fig. 2 ANSYS Mesh Results of 2D Sphincter Airflow Simulations

As depicted in the visualization, the mesh reveals a discernible pressure gradient spanning the tower. Throughout the simulation, the tower undergoes inflation from its top section to the lower sections, accounting for gravitational effects and backflow dynamics. The high pressure above the inlet is indicated by the intense red referencing the heavy accumulation of air within the initial section, progressively decreasing in subsequent sections. Though the pressure values may not precisely mirror real-world conditions, they effectively illustrate the trend of diminishing pressure with each successive section during tower deployment, thereby validating the concept's feasibility.

A visual graphical rendering of the pathlines was generated from the same simulation presented above. These pathlines, as shown below in Fig. (3) illustrate the movement of air throughout the tower.

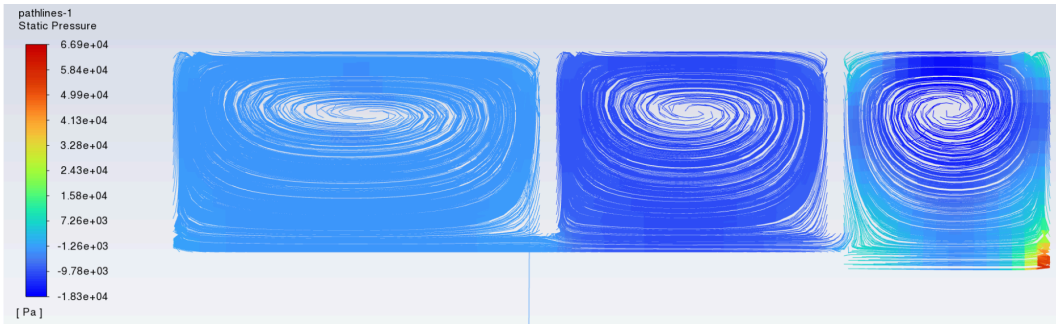

Fig.3 ANSYS Pathline Results of Sectional Airflow Simulations

As seen in the figure, the air quickly fills up the initial space, eventually being bottlenecked at each sphincter. Within these sections, turbulence disrupts the airflow, posing challenges to smooth progression from one section to the next. These airflow peculiarities serve to reinforce sectional inflation, contributing to the overall deployment process given at the expense of time.

In summary, the simulation results provide compelling evidence supporting the functionality and effectiveness of the sectional inflation system in promoting stable deployment and structural integrity of space-grade towers. These findings validate the original design concept and provide proof-of-concept for the small-scale prototype that is being manufactured.

C. Power and Electrical Subsystem

Equation (6) was utilized to simulate the system's average power consumption over time, incorporating various microcontroller delay scenarios in MATLAB. The resulting graph depicted fluctuations in power draw influenced by the ratio of active and idle modes. Specifically, the active mode exhibited a positive linear trend, while the idle mode demonstrated a negative linear trend when graphed against the subsystem average power draw versus time spent in consumption mode.

The capacitance simulation results reveal that a 24V battery with a 400Ah capacity effectively meets HAMSTIR's requirements. The simulation indicates an inverse relationship between normalized battery capacity and cost, justifying the selection of moderate voltage batteries (12V, 24V, and 48V). Analysis of battery capacity depletion over a lunar night cycle shows that the 24V battery maintains a healthy 90Ah reserve, ensuring reliability amid increased power demands or battery degradation. Additionally, the battery capacity fluctuation over five life cycles yields a calculated life cycle of 19.4 days, providing sufficient power through lunar nights.

Equations (12) and (13) were used to analyze the solar panel power generation throughout the lunar day cycle. The evaluation showed that for the HAMSTIR's space-grade panels, which are estimated to have a 30% efficiency rating, a total power rating of about 100W is required, translating to roughly 25W per solar panel. Over the 354-hour lunar day cycle, the panels are anticipated to produce 30W of power output. This surplus ensures adequate power reserves to accommodate potential disruptions such as loss of area coverage, solar cell damage, or sunlight blockage.

D. Structures and Mechanisms Subsystem

Initial proofs of concept relating to the HAMSTIR tri-slot design were created using SOLIDWORKS. The full-scale and prototype designs were initially modeled and then the concatenation and deployment of the slot-bearing supports was successfully demonstrated through mechanical simulation. The full-scale model, as seen to the right in Fig. (4), was then selected to be Aluminum 6061-T6 for both the basebox and tri-slot due to the benefits relating to strength and low mass. The material for the prototype tri-slot was determined to be ABS filament for equivalent purposes and additional ease of manufacturing while the basebox was converted to plexiglass. The full-scale system was designed with eight tri-slot sections, a collapsed height of 1.67 feet, an extended height of 23.9 feet, and mass of 165 kg. The prototype design was adjusted for manufacturing purposes to not include the indented basebox section for the tri-slots containment. The prototype was also limited to three sections, features a collapsed height of 13 inches, an extended height of 68 inches, and a mass of 12 kg.

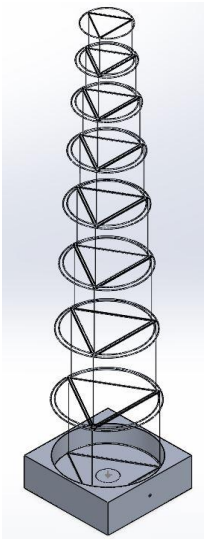

ANSYS was then used to simulate the loads and conditions that will be endured by both the HAMSTIR full-scale design and prototype in their respective environments. Valuable information such as stress and deformation were derived from these simulations. Full-scale tests

included the model experiencing the acceleration of a rocket launch and bearing the load of the communications equipment under the Moon's gravitational pull. Prototype simulations focused on weight bearing the prototype's reduced communications load under Earth's gravity. Each simulated value was exaggerated to incorporate a factor of safety into the simulations.

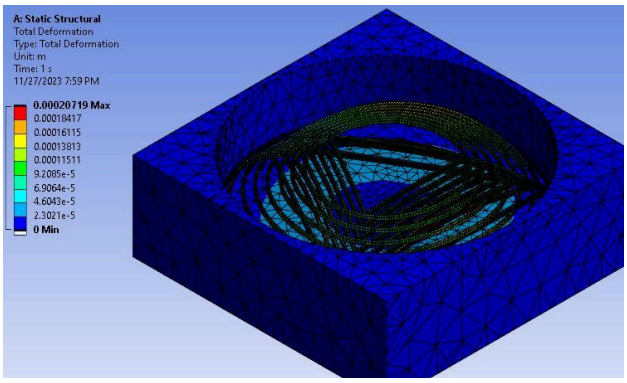

Fig. 5 Deformation of Full-Scale Design under Launch Acceleration

The potential acceleration experienced during launch for the collapsed full-scale HAMSTIR was exaggerated to be 40 m/s^2. Under these conditions, the full-scale design experiences a maximum deformation of around 2 mm, focused on the uppermost layers of the tri-slot as apparent by Fig. 5. Simulations upon the lunar surface for deformation and stress were also conducted, featuring an extremely exaggerated 200 N communications load to show the strength of the tri-slot design. In Figs. (6a) and (6b), the maximum amount of deformation was found to be 1.5 mm and the maximum stress was found to be about 2.49e7 Pa, both focused along the top section of the tri-slot. Each of these derived values were found to be very minimal and suggest the strength of the HAMSTIR's full-scale design.

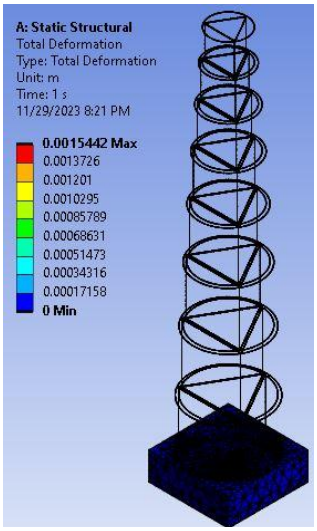

a) Full-Scale Model Deformation With Moon Gravity & 200N Load

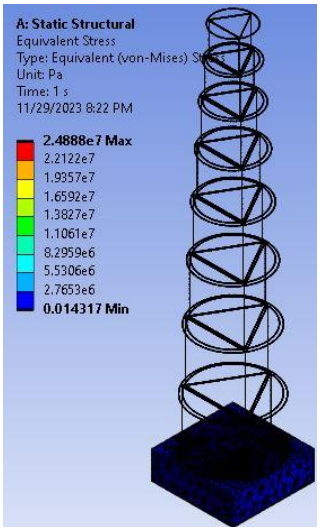

b) Full-Scale Model Stress With Moon Gravity & 200N Load

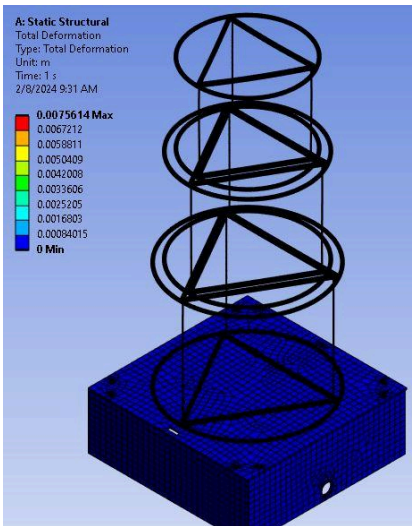

c) Prototype Deformation With Earth Gravity & 64N Load

Fig. 6 Deformation and Stress Results of Full-Scale and Prototype Under Moon and Earth Gravity and Loading

The prototype design was only tested for its ability to bear the communications load under Earth's gravity. The prototype communications load was greatly exaggerated to be 64 N, and as can be seen in Fig. (6c) the maximum deformation was found to be 7.5 mm for this design primarily focused on the top layer of the tri-slot. While this

deformation is significantly larger than the full-scale's results, deformation readings are cumulative through each portion of the model. This means that deformation readings are not read based on the individual deformation of a single part of the design, but rather the attributed deformation of the entire model. The prototype experienced slightly more flexing occurring in each individual pole, each slightly adding to the maximum deformation readings within the top section. With the exaggerated communications load and this fact in mind, security in the HAMSTIR prototype's structural stability can be assured.

E. Thermal, Radiation, and Survivability Subsystem

The outermost layer of the HAMSTIR's inflatable portion will be constructed using Kapton, a material known for its resilience in extreme temperatures ranging from -269℃ to 400℃. Kapton has an ultimate tensile strength of 231 MPa. As shown in the figure below, at a temperature of 325℃, almost three times the maximum temperature on the moon, it would take over 41 days for the tensile strength of the material to reduce to 0%. Renowned for its electrical insulation properties and resistance to heat and UV, Kapton has been widely utilized by NASA in various space missions, including Mars rovers, the Hubble Space Telescope, and the Parker Solar Probe.

Nextel, a ceramic fiber renowned for its durability, will serve as the second layer. Developed by 3M, Nextel can withstand temperatures exceeding 1000℃ and maintains 100% of its tensile strength even at temperatures as high as 700℃. Its low coefficient of thermal expansion makes it ideal for aerospace applications, and it has been used in spacecraft heat shields and thermal protection systems.

The third layer, composed of Kevlar, specifically Kevlar 49, offers exceptional tensile strength of approximately 3.6 GPa. With a density of 1.45 g/cm^3 and high resistance to temperatures exceeding 400℃, Kevlar has been extensively employed by NASA in spacecraft heat shields, spacesuits, parachute cords, and suspension lines for its remarkable strength-to-weight ratio and protective properties against micrometeoroid impacts, extreme temperatures, and radiation.

The innermost layer of the HAMSTIR full-scale model comprises a silicone bladder, chosen for its ability to retain air effectively. Silicone, known for its lightweight properties with a density ranging from 1.1 to 1.3 g/cm^3, exhibits considerable stretchability before breakage, with an elongation at break ranging from 200% to 700%. Its low porosity, typically ranging from less than 1% to 5%, makes silicone an ideal choice for air retention and insulation. NASA has extensively utilized silicone elastomers for seals, gaskets, and O-rings in spacecraft to ensure airtight and watertight seals, as well as for joints and bellows to accommodate movement and thermal expansion.

To evaluate the feasibility and endurance of the HAMSTIR towers, ANSYS computational fluid dynamics software was utilized to assess the thermal and radiation characteristics of its outer materials, Kapton and Nextel, under lunar surface temperatures. Transient thermal analyses were conducted across the lunar day cycle, considering radiation as a thermal load. The results indicated uniform temperature distribution and moderate heat flux for both materials, ensuring effective temperature control and thermal insulation. Additionally, MATLAB was employed to analyze the tensile stress of Kevlar against daily micrometeoroid impacts, confirming its suitability for withstanding lunar surface debris. Reflective coating simulations were performed using Fresnel equations to assess material reflectance, demonstrating high reflectance levels, especially at sunset and sunrise angles, making it an effective solution for solar array reflection. This comprehensive analysis underscores the durability and reliability of the HAMSTIR under lunar conditions.

IV. Discussion

The HAMSTIR's iterative process of small-scale prototype testing and full-scale modeling has successfully validated its design concepts. ANSYS simulations demonstrated the feasibility of the sectional inflation system, visualizing pressure gradients and airflow dynamics that promote stable deployment and structural integrity. The simulations also provided proof of the reliability and applicability of findings across scales.

MATLAB simulations highlighted the communication subsystem's capability for adequate antenna isolation, extended signal coverage over significant distances for robust lunar surface connectivity, and optimized moment balance through center of mass alignment. Power subsystem analyses determined average power consumption, battery capacity, solar panel efficiency, and charge-discharge cycles to ensure efficient operation during lunar day-night cycles.

Structural analyses through SOLIDWORKS and ANSYS offered insights into stress distribution, deformation, and load-bearing capacities under lunar and Earth conditions, guiding material selection like Aluminum 6061-T6 and ABS filament for balancing strength, mass, and manufacturability. Thermal and radiation analyses emphasized robust outer layer materials like Kapton, Nextel, Kevlar, and silicone to protect against temperature variations, radiation exposure, and micrometeoroid impacts, confirming their thermal stability, radiation resistance, and reflectance properties.

Overall, the comprehensive analyses and simulations offer valuable insights for the ongoing development and optimization of the HAMSTIR system, demonstrating significant progress towards enhanced communication capabilities and support for future lunar missions.

V.Conclusion

The HAMSTIR project represents a groundbreaking leap in lunar communication infrastructure, addressing the critical need for robust and reliable connectivity on the Moon while still maintaining a low volume-weight ratio. Through a multidisciplinary approach integrating inflatable structures, telecommunications, power systems, structural mechanics, and thermal considerations, HAMSTIR offers innovative solutions to the challenges of establishing communication networks in extraterrestrial environments.

The methodology employed in the design and analysis of HAMSTIR highlights the meticulous attention to detail and the rigorous testing protocols implemented to ensure its feasibility and performance under simulated lunar conditions. From the comprehensive analysis of the communications subsystem to the structural integrity assessments of the inflation subsystem and the detailed evaluation of power management and thermal resistance, every aspect of HAMSTIR's design has been critically examined and refined to meet the demands of lunar exploration missions.

Central to the success of HAMSTIR is offering an inexpensive, efficient, and reliable option that enables astronauts and rovers to communicate and facilitate the exchange of critical data and information. HAMSTIR extends the potential reach of future terrestrial communication networks on the Moon, laying the groundwork for enhanced connectivity and support for future lunar exploration endeavors.

The small-scale prototype of HAMSTIR is currently in the process of being manufactured and is expected to be fully functional by the end of March 2024. Further analysis and testing will be conducted to validate its performance and ensure the design readiness for possible deployment for future lunar missions.

In conclusion, the HAMSTIR project exemplifies the spirit of innovation and collaboration driving sustainable space exploration forward. As humanity continues to push the boundaries of exploration and discovery, projects like HAMSTIR play a pivotal role in advancing our understanding of the cosmos and expanding our presence beyond Earth. With its innovative design, robust performance, and transformative potential, HAMSTIR heralds a new era of lunar communication infrastructure and inflatable technology, paving the way for humanity's continued exploration and discovery in the vast expanse of space.

References

[1] Litteken, Douglas A. “Inflatable Technology: Using Flexible Materials to Make Large Structures.” NASA NTRS, NASA, ntrs.nasa.gov/api/citations/20190001443/downloads/20190001443.pdf. Accessed 26 Sept. 2023.

[2] Gruber, Petra. "Deployable structures for a human lunar base." Acta Astronautica, 2007, April 19. https://www.sciencedirect.com/science/article/pii/S0094576507000690.

[3] "Composite overwrapped pressure vessels (COPV) - NASA technical reports ..." NASA. https://ntrs.nasa.gov/api/citations/20110008406/downloads/20110008406.pdf.

[4] NASA. "Communications and the Lunar Outpost." NASA. https://www.nasa.gov/pdf/514478main_AL_ST_Comm_FINAL.pdf.

[5] "Repeater Tower - Deployable Mobile Coverage Tower." R-Spectrum. r-spectrum.com.au/systems/repeater-tower-deployable-mobile-coverage-tower. Accessed 27 Oct. 2023.

[6] "What Is a Bi-Directional Amplifier (BDA)?" B.C. Communications Inc. bccommunications.ca/blogs/resources/bi-directional-amplifiers. Accessed 27 Oct. 2023.

[7] "Everything RF." Everything RF, 4 May 2022, www.everythingrf.com/community/what-is-a-yagi-antenna.

[8] "Antenna 2.4ghz / 5ghz Sector Box 15dbi 2V 5H." Axuse Group. axuse.com/lte/2-4-ghz-antennas/antenna-2-4ghz-and-5ghz-sector-box-2x2-mimo-15dbi-2v-5h.html. Accessed 27 Oct. 2023.

[9] "Cradlepoint Multi-Band Omni-Directional Outdoor Antenna 4G LTE 5G - 170668-000." JEFA Tech. www.jefatech.com/products/170668-000. Accessed 27 Oct. 2023.

[10] SignalBooster.com. "Differences Between 3G (1x) vs. 4G LTE Signal Strength in dBm." SignalBooster.com, www.signalbooster.com/blogs/news/differences-between-3g-1x-vs-4g-lte-signal-strength-in-dbm.

[11] IEEE Xplore. "Cellular Signal Enhancement in an Indoor Environment Using Directional Antennas." IEEE Xplore, ieeexplore.ieee.org/document/6929535.

[12] MIT Computer Science and Artificial Intelligence Laboratory. "Cellular Repeater Placement Outside Buildings." MIT CSAIL,people.csail.mit.edu/bkph/cellular_repeater_outside.shtml#:~:text=(5)%20Base%20station%20(cell,receiving%20antenna%20should%20be%20mounted).

[13] Gao, X., & Li, L. (2012). "Research on RSSI in Received Signal Strength Indication Positioning." 2012 International Conference on Systems and Informatics. https://ieeexplore.ieee.org/document/6317307.